

# Comparison of Seismic Reflection and Ground-penetrating Radar Imaging at the Controlled Archaeological Test Site, Champaign, Illinois

J. A. HILDEBRAND,<sup>1\*</sup> S. M. WIGGINS,<sup>1</sup> P. C. HENKART<sup>1</sup> AND L. B. CONYERS<sup>2</sup>

<sup>1</sup> Scripps Institution of Oceanography, University of California San Diego, La Jolla, CA 92093-0205, USA

<sup>2</sup> Department of Anthropology, Denver University, Denver, CO, USA

**ABSTRACT** Shallow seismic reflection and ground-penetrating radar images were collected at a replicated burial mound in the Controlled Archaeological Test Site (CATS) in Champaign, Illinois. The CATS mound contains a pig burial within a wood-lined crypt at a depth of 1.6–2.4 m. Seismic reflection data were collected from two different energy sources: a small (0.5 kg) hammer for an impulsive source, and a vibrator for a frequency swept source. Seismic data were collected at densely spaced points (5 cm) along a line of 48 geophone receivers. These data were stacked in a common mid-point gather, band-pass filtered, and processed with frequency–wavenumber migration. The seismic image produced by the hammer source was dominated by bodywaves at 120 Hz, whereas the vibrator source image was dominated by surface waves at 70 Hz. Both seismic sources revealed clear reflections from the burial crypt, and placed the top of the crypt at the correct depth with a seismic velocity of 120 m s<sup>-1</sup>. The bottom of the crypt was poorly defined by the seismic data owing to multiple reflections within the crypt. The vibrator source also revealed a high-frequency (360 Hz) reflector at 2.7 m depth within the mound, perhaps due to a resonant cavity within the pig's body. Single channel ground-penetrating radar data were processed with the same approach, including band-pass filtering and migration. The radar data reveal clear reflections from the burial crypt. Extremely fast radar velocities (260 mm ns<sup>-1</sup>) are required in the upper portion of the burial mound to place the top of the crypt at its correct depth. The bottom of the crypt was well defined by ground-penetrating radar, and was located accurately with respect to the top of the crypt with a moderate radar velocity (170 mm ns<sup>-1</sup>). The application of both seismic reflection and ground-penetrating radar to the same site may be beneficial for improved understanding of their abilities for shallow subsurface imaging. Copyright © 2002 John Wiley & Sons, Ltd.

*Key words:* seismic reflection; ground-penetrating radar; burial mound

## Introduction

Reflection imaging methods hold great promise for investigating buried cultural resources (Steeple and Miller, 1990; Conyers and

Goodman, 1997). Reflection imaging can provide information on the depth of buried objects and structures as well as their position within a site. A comparison is presented between two geophysical prospecting methods based on reflection imaging in shallow soil: seismic reflection imaging (SRI) and ground-penetrating radar (GPR). Seismic reflection and GPR imaging methods are similar in that both are based

\* Correspondence to: J. A. Hildebrand, Scripps Institution of Oceanography, University of California San Diego, CA 92093-0205, USA. E-mail: jhildebrand@ucsd.edu

upon wave propagation through the soil, and upon wave reflection from buried objects or structures. They are different in the type of waves used for imaging—seismic or radar—making for differences in the efficiency of wave coupling, propagation and reflection.

Application of SRI and GPR at the same site will improve our understanding of these methods for imaging buried objects or structures. In this paper, we apply SRI and GPR at the Controlled Archaeological Test Site (CATS) in Champaign, Illinois, where a range of buried objects and features have been constructed to simulate prehistoric cultural resources typical of the central USA (Isaacson *et al.*, 1999). We imaged a simulated burial mound, incorporating a pig within a wood-lined crypt at a depth of 1.6–2.4 m. Both the SRI and the GPR systems detected clear reflections from the burial crypt. By applying seismic and radar techniques together at a setting with known buried objects and structures, we provide an evaluation of the relative imaging characteristics of these two approaches.

## Background

Geophysical reflection imaging uses the same experimental geometry, whether seismic or radar waves are used as the energy source. In both cases, the sources and receivers are located at the ground surface. An energy pulse is transmitted into the ground, and is returned to the surface as a series of reflections from discontinuities at depth. The reflected energy is received at one or more locations along the ground surface, at near normal incidence angles. Data are collected as reflected energy versus time, and converted to depth using knowledge of the propagation velocity within the soil. To construct images of the subsurface reflectors, the sources and receivers are moved along the ground surface. The resolving power for reflection imaging is limited by the wavelength of the energy source, which is controlled by the wave frequency and propagation velocity. Attenuation and scattering increase for short wavelength energy, placing practical limits on the highest frequencies that may be used, and therefore, on the overall imaging resolution.

Ground-penetrating radar uses radio frequency electromagnetic waves as an energy source, which are sensitive to the dielectric properties of the soil and reflective objects within it. The principal factors effecting soil dielectric properties are clay composition, compaction and water content. Increased water content results in lowered wave velocity (Topp *et al.*, 1980). The presence of electrically conductive clay or alkaline soils results in high GPR energy attenuation, and limits the depth of its penetration into the ground (Olhoeft, 1986). The GPR resolving power is also limited by the wavelength of the electromagnetic energy; operating in the 100–1000 MHz frequency range, typical radar velocities in soil are  $150 \text{ mm ns}^{-1}$ . The corresponding radar wavelengths for soil imaging are 0.15–1.5 m, which determines the resolution of detectable features. These wavelengths may attenuate at 2–30 dB per metre in soils, depending upon their composition and water content (Olhoeft, 1986).

One advantage of GPR over SRI is that radio frequency electromagnetic waves are easily coupled to the soil by placing the antenna at or near the ground surface. The antenna systems used for GPR can be moderately sized, allowing them to be easily transported for rapid data collection. Under good field conditions, GPR is capable of mapping up to 5000 m<sup>2</sup> areas on a 0.5 m grid spacing during one day in the field. These gridded GPR data can be processed into depth slices, mapping the radar reflectivity of buried surfaces (Goodman *et al.*, 1995).

Imaging with acoustic or seismic waves has a proven capability when used for medical diagnosis, undersea mapping and oil exploration (Claerbout, 1985). Only relatively recently has seismic reflection or acoustic imaging been applied to soils at depths of 10 m or less (Steeple, 1998; Baker *et al.*, 1999; Frazier *et al.*, 2000). Conventional seismic and acoustic techniques must be modified to account for the properties of shallow soils.

A key parameter for SRI is that several propagation modes may be present: longitudinal (P-waves), shear (S-waves) and surface waves. P-waves have particle motion in the direction of propagation; S-waves have particle motion transverse to the propagation direction; and surface waves are trapped at the ground surface

with retrograde-elliptical particle motion. Each of these modes will have a distinct propagation velocity in soil, although in general the P-wave velocity will be more than twice that of the S-wave or surface wave velocity.

Seismic waves used for reflection imaging are sensitive to the elastic properties within the soil. The principal factors effecting soil seismic velocity are its composition (e.g. grain size), water content, and the confining pressure (Stoll, 1989). Typical values for P-wave velocity in the upper few metres of soil are 180–250 m s<sup>-1</sup> (Steeple, 1998; Baker *et al.*, 1999). At frequencies of 100–1000 Hz, associated seismic wavelengths are 0.2–2 m. These wavelengths set the resolution that may be attained by seismic imaging systems. Likewise, these wavelengths may attenuate at 1–10 dB m<sup>-1</sup> depending on soil composition and water content.

The radar or seismic reflectivity of a buried object or structure is an important consideration for how well it may be imaged. Reflectivity is set by the impedance contrast between the object and the surrounding media, in this case soil. Reflection coefficients, the ratio of reflected to incident wave amplitude, may be large for certain objects; for instance, a buried cavity would be essentially perfectly reflective for seismic waves. Impedance variations associated with soil composition or water content also may reflect radar or seismic energy. For example, the reflections at the boundary between two soil layers of slightly different composition may be of the order of a few per cent. Combining efficient propagation through the soil with a highly reflective object will produce a reflection from a buried object or soil layer that has a detectable return at the ground surface. Total losses between transmitted and reflected signals of 50 dB or more are typical for the signals seen by a reflection imaging system.

#### *A shallow seismic reflection imaging system*

The primary problem for adapting SRI to shallow depths within soils is twofold: (i) the need to produce high frequency seismic energy, and (ii) the need to effectively couple the seismic

source and receivers to the soil. In the typical settings for SRI—oil exploration, oceanography and medical imaging—sensors are easily coupled to the media, and the media allows for efficient propagation. Shallow soil presents greater difficulties for coupling, and it is a complex media for seismic propagation.

We designed an SRI system suitable for imaging at shallow depths in soils. The system used a series of closely spaced geophones, deployed in a line along the surface of the ground, and near these geophones, a series of seismic sources or shots. A digital seismograph allowed large dynamic range signal recordings. To enhance the geophone-to-ground coupling, we watered each geophone, just prior to each shot. With successive shots the geophone array was translated along the line to maintain a constant geometry between the shot and the receiver positions. To enhance seismic source coupling to the ground, we inserted a short pipe into the ground at each shot point. Two different energy sources were directed at the pipe: an impulsive source was created by striking the pipe with a 0.5 kg hammer, and a controlled vibrator source was created by attachment of a commercial shake table to the pipe. The signal generated by each method was repeated multiple times at each shot point and stacked within the seismograph.

There may be several advantages to using a controlled vibrator source for high-resolution shallow seismic imaging. The controlled vibrator source allowed a variety of waveforms to be generated; in particular, we used swept frequency waveforms, which increased logarithmically in frequency with increasing time. The vibrator source allowed efficient generation of high-frequency seismic energy. The frequency content of typical impulsive seismic sources, such as weight drops and sledgehammer or shotgun sources, may be limited in the high frequencies needed for high-resolution shallow imaging. Further, there may be problems in gaining permission to use such sources in urban areas, or sensitive site areas. Unlike impulsive sources, the frequency content and the source strength can be defined independently for the vibrator source. The vibrator signal also can be adapted to specific site conditions, such as

the quality of source coupling. For a given source strength, because the energy density for a vibrator source is less than for an impulsive source, vibrator sources are non-destructive, do not produce non-linear excitation of the soil, and are less likely to overdrive the seismic receiving system. The signal detection for a vibrator source can be done as a cross-correlation between transmitted and received signal. This allows for significant signal strength gain (product of the signal time and bandwidth), which provides better protection against ambient site noise.

The key system elements of the controlled vibrator source are a signal generator—set to transmit a frequency swept signal—a power amplifier and the portable vibrator. The entire system is powered using conventional 12 V car batteries and a dc-to-ac power inverter. The portable vibrator generates force using an electromagnet system; there is a magnetic armature within a system of coils. When current is passed through the coils the armature can generate up to 23 kg of peak force with a maximum stroke of 1.3 cm peak-to-peak. The vibrator weighs 39 kg and has dimensions of 25 × 25 × 30 cm, allowing it to be field portable. The vibrator is capable of generating any kind of frequency swept signal (linear, log, etc.) in the frequency range 2 to 10 000 Hz. To couple the vibrator to the ground we first drive a 1 inch pipe into the soil, and then screw the vibrator on to the pipe by a tapered coupling. An external suspension, consisting of a beryllium–copper cross-spring keeps the armature in the centre of its driving range when the vibrator is attached to the pipe. In practice the usable frequency range is 20 to 3000 Hz, limited on the low end by the mass of the vibrator (motion of the vibrator dominates) and at the high end by attenuation and resonance of the spring and support structure. A signal generator is programmed for the appropriate frequency band and type of sweep (e.g. log). The signal generator drives a power amplifier with a 250 W output, which then drives the vibrator. To monitor vibrator motion an accelerometer was mounted on the pipe, just below its coupling with the vibrator, and the accelerometer output was recorded as a channel on the digital seismograph.

### The controlled archaeological test site

As a venue for testing these approaches for shallow seismic imaging we chose the Controlled Archaeological Test Site (CATS), a simulated archaeological site in Champaign, Illinois (Isaacson *et al.*, 1999). The CATS facility replicates features present in some North American archaeological sites under a controlled environment. This site is located on a level plot of silty clay and silt-loam soils, in a former agricultural field. The soil profile has an A horizon measuring about 36 cm in thickness, and a B horizon of about 84 cm thickness. Preliminary surveys and site records indicate no previous prehistoric or historic disturbance, other than farming. Features constructed at the CATS facility include: monumental and domestic architecture; pig and dog burials in mounds, under house floors, and in isolated pits; and hearths, roasting pits and artefact clusters.

We chose to image a circular mound feature in the central portion of the CATS site that simulates mortuary features found in Midwest archaeological sites (Figure 1). Previous studies have demonstrated that reflection imaging is an efficient means for investigating burial mounds (Goodman and Nishimura, 1993). The CATS burial mound surface is about 7 m in diameter and 1.4 m in height. To construct the mound, the soil within the plough zone was stripped to a depth of 0.2 m over a circular area 7 m in diameter. In the middle of the stripped area, a pit was excavated, extending to a depth of 0.7 m beneath the plough zone level. The pit dimensions were rectangular, measuring 1.8 m in the north–south direction and 1.2 m in the east–west direction. To form a burial crypt, the sides of the pit were lined with wooden logs and an extended pig was placed in it, along with four ceramic vessels and freshwater mollusc shells. Pig burials are a good simulation for human burials (France *et al.*, 1992). The wooden logs lining the sides of the burial crypt were sycamore tree limbs, measuring up to 10 cm in diameter and piled up to 25 cm above the plough zone base level.

A secondary burial pit was excavated about 2 m to the southeast of the mound centre, extending to a depth of 0.16 m beneath the plough zone.

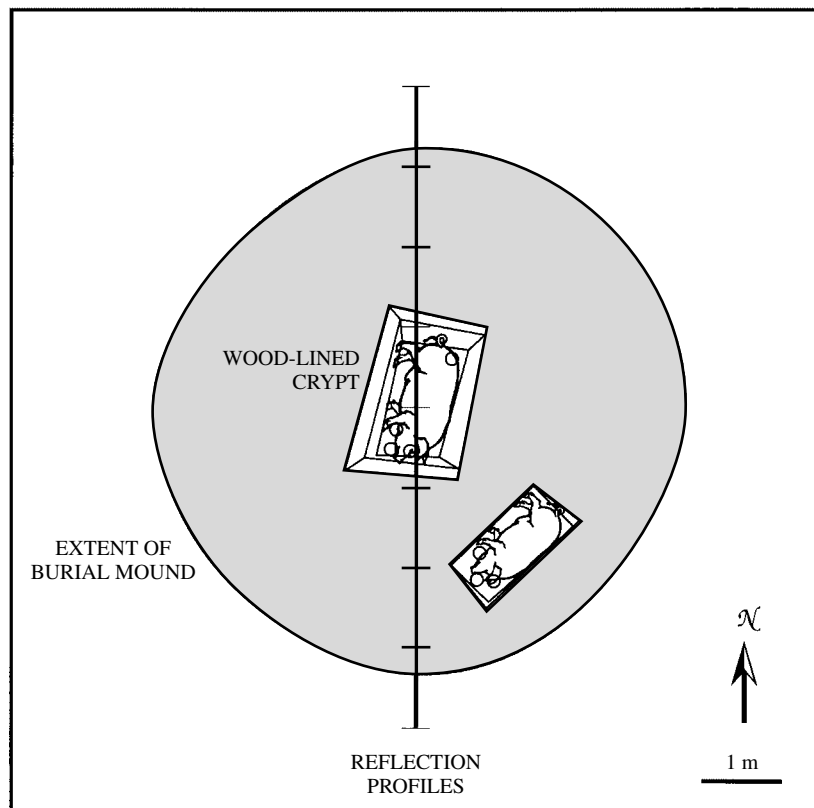


Figure 1. The CATS burial mound is shown in map view with the reflection profile (1 m ticks) crossing the centre of the mound. The mound surface is about 7 m in diameter (shaded circle). A wood lined crypt, containing a pig burial and four pottery vessels, is located at the centre of the mound. A secondary pig burial with three pottery vessels is located about 2 m to the southeast of the mound centre.

This pit was 1 m long and 0.5 m wide, orientated with its axis along a northeast–southwest line. A pig was also placed in this burial pit, along with three ceramic vessels and mollusc shells.

Both the crypt and the secondary burial pit were filled with A horizon soil stripped from the plough zone. At its centre, the mound was built to a height of 1.4 m above the ground level, using first local A horizon soils and then A horizon soils that were imported to the site. These burial features were constructed in 1997, about one year before we imaged the site in October 1998.

#### *Seismic reflection imaging at CATS*

To determine how well the burial crypt and other mound features could be imaged, a seismic reflection line was acquired in a north–south direction across the centre of the CATS burial mound.

Using a 48-channel Geometrics Strataview (40 Hz geophones, 24-bit A/D, 32 KHz sample rate), seismic receivers were placed at 5-cm intervals along the line. All shots were located in the middle of the geophone spread, where a 10-cm geophone spacing was provided. The shots were displaced 5 cm to the east of the geophone line to avoid disturbance to the geophone plantings. After each shot the entire line of geophones was translated 20-cm north, giving a 20 cm shot interval. There were a total of 38 shot points in the burial mound reflection line. The line was about 8 m in total length and required 8 h in the field to collect.

Two seismic sources were used at each shot point: a hammer impulsive source and a vibrator swept frequency source. Either source was coupled to the ground through a 1 inch diameter, 1 foot long, steel pipe. A sledgehammer was used to drive the pipe about 6 inches into the ground, typically requiring four to eight blows.

A 0.5 kg hammer was then struck on the top of the pipe for 15 blows, and these data were stacked by the Strataview and saved as a 0.250 s record. The vibrator source was then screwed on to the top of the pipe and a logarithmically frequency swept signal (1–1000 Hz) of 1 s duration was transmitted for 15 repetitions, stacked by the Strataview and recorded as a 1.250 s record. By using a vibrator signal with a frequency that increased logarithmically with time, an extremely broadband energy spectrum was produced, without placing excessive emphasis on the highest frequencies. Within this frequency sweep, time is divided equally between frequency bands at 1–10 Hz, 10–100 Hz and 100–1000 Hz. In practice, the vibrating source is inefficient at the lowest frequencies (1–10 Hz), but including these frequencies allows a smooth beginning to the signal.

The data were checked for their quality during and after the field acquisition. Data were processed on a computer workstation using the SIO-SEIS software package (<http://sioseis.ucsd.edu>). Field records were converted into a single SEG-Y file for each source type. Shot gathers were examined for data quality, for example, bad cable connections between the geophone and the recording unit, and for the presence of reflection events. Vibrator data were cross-correlated using the closest geophone to the shot point (about 7 cm separation) as the reference trace.

A shot gather from the hammer source, located at the centre of the mound, is shown in Figure 2. The fastest waves are air coupled, travelling at  $335 \text{ m s}^{-1}$  with a linear moveout, that is, arrival time versus source–receiver separation. The first ground-coupled arrivals are associated with P-waves, travelling either as direct or as shallow refracted energy at velocities of about  $100 \text{ m s}^{-1}$ . These can be seen at  $\pm 1 \text{ m}$  offset with about 10 ms delays. The surface waves, which have a linear moveout, are seen at  $\pm 1 \text{ m}$  offset and about 17–20 ms delay, suggesting a velocity of about  $55 \text{ m s}^{-1}$ . Some near-source geophones in Figure 2 ( $\pm 0.7 \text{ m}$ ) show a clipped signal at near-origin times (0–40 ms). This suggests that the impulsive source overdrove the seismic receiver at these times and locations, primarily due to large surface wave signals.

The same shot gather is shown in Figure 3, filtered in two different frequency bands and

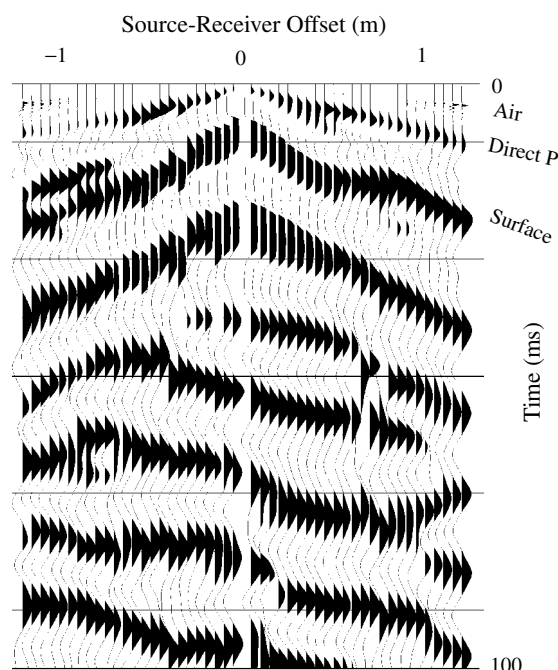


Figure 2. Shotpoint gather of seismic data collected with a 0.5 kg hammer source, located near the centre of the CATS burial mound with geophone receivers aligned in a north–south direction. The air coupled wave, direct P wave, and surface wave are denoted. This and all subsequent seismic plots use a 10 ms AGC display window.

with the clipped portions of the signal surgically muted. Air coupled waves are most apparent at high frequency. At 45–51 ms, a high frequency reflection with hyperbolic moveout is seen near normal incidence (Figure 3b). Likewise, at low frequencies, complex reflection events appear at 40–100 ms (Figure 3a).

A shot gather from the vibrator source, positioned near the centre of the mound, is shown in Figure 4. Surface waves with frequencies near 100 Hz dominate the early arrivals, travelling at velocities of about  $55 \text{ m s}^{-1}$ . At frequencies near 360 Hz, a series of reflecting events may be present at 50–100 ms (Figure 4b).

Shot gather data were sorted into common midpoint (CMP) gathers for further processing; the goal of a CMP gather is to display signals originating from a common reflector, but with varying shot–receiver separation. Reflection events in a CMP gather will typically appear with hyperbolic moveout. Retaining only geophones in the inner 1.2 m, and using the geometry described above,

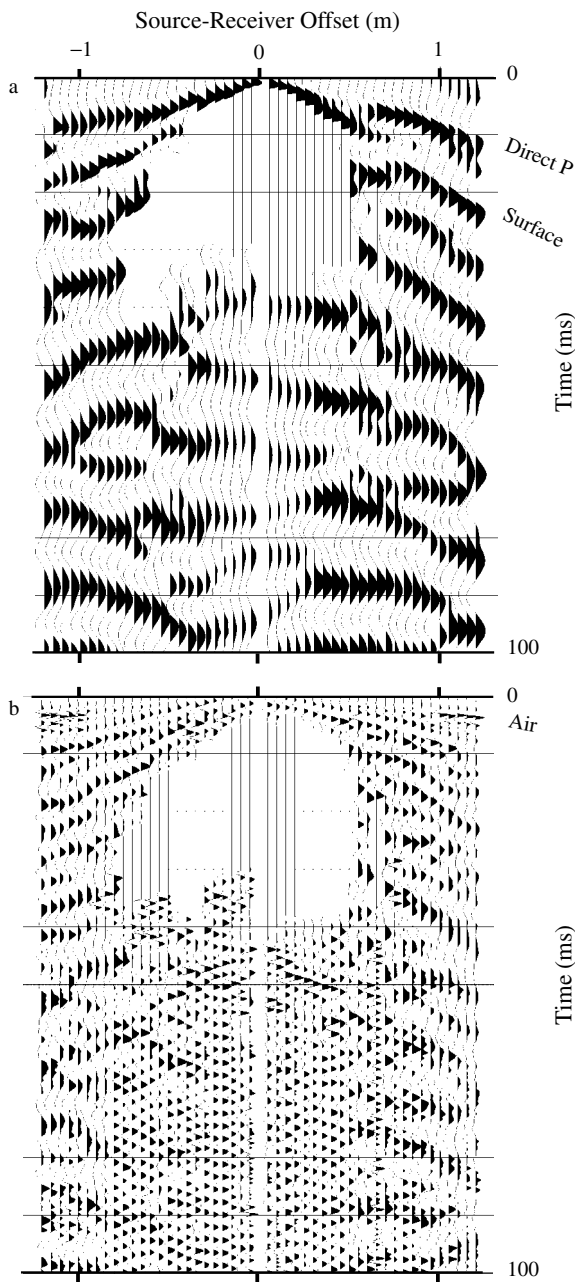


Figure 3. Shotpoint gathers of the same data as in Figure 2, with clipped data muted for two different band-pass filters: (a) 100–800 Hz and (b) 600–1000 Hz.

CMP gathers yield threefold data at the minimum mid-point spacing of 2.5 cm. For purposes of velocity analysis, 12-fold data were examined with 10-cm mid-point spacing. A series of uniform velocities were tested for stacking the CMP

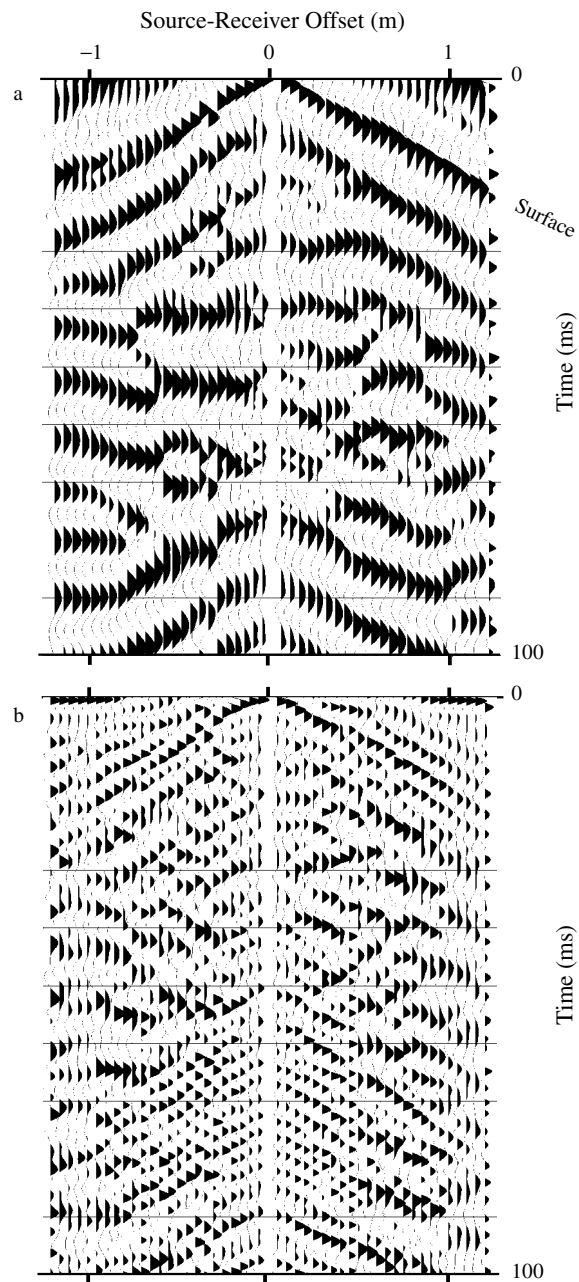


Figure 4. Shotpoint gathers of seismic data collected using a vibrator source with a 1–1000 Hz logarithmic sweep. The data are presented with two band-pass filters: (a) 100–800 Hz and (b) 320–400 Hz. The source and receiver locations are the same as in Figure 2.

gathers; a velocity of 120 m s<sup>-1</sup> gave the best results, that is, the best summation or stacking of subsurface reflectors. We applied this velocity for all depths within the seismic section. The

mound topography was applied as a static shift to the seismic data and a 10-ms automatic gain control (AGC) window was used for display. Geophone channels were muted where their data were noisy or clipped from the large amplitude of the impulsive source.

The seismic reflection image produced by the hammer source has a dominant frequency of about 120 Hz (Figure 5a). At the edges of the mound, relatively flat-lying arrivals are seen for all times in the section. The uppermost of these arrivals (surface to 20 ms) has a lower frequency content than arrivals beneath it. This frequency inversion with depth (low frequency above high) is consistent with the arrival being refracted rather than reflected energy (Steeple and Miller, 1998). Within the mound interior are a series of reflection events that have their

greatest strength and are shallowest beneath the mound centre. A frequency–wavenumber migration (Stolt, 1978; Hatton *et al.*, 1986) was applied to these data to improve the reflector definition, assuming a velocity of  $120 \text{ m s}^{-1}$  (Figure 5b). An improved focusing of reflected energy is seen in the migrated image, for instance, vertical discontinuities in the reflections are seen at  $x = -0.9 \text{ m}$  and  $1.2 \text{ m}$  in the migrated image (Figure 5b), whereas these areas have hyperbolic energy tails in the non-migrated image (Figure 5a).

The seismic reflection image produced by the vibrating source using a log sweep is shown in Figure 6. The dominant frequencies are at about 70 Hz, although higher frequencies (360 Hz) are observed in some portions of the image. At the edges of the mound, the arrivals tend to follow the mound topography.

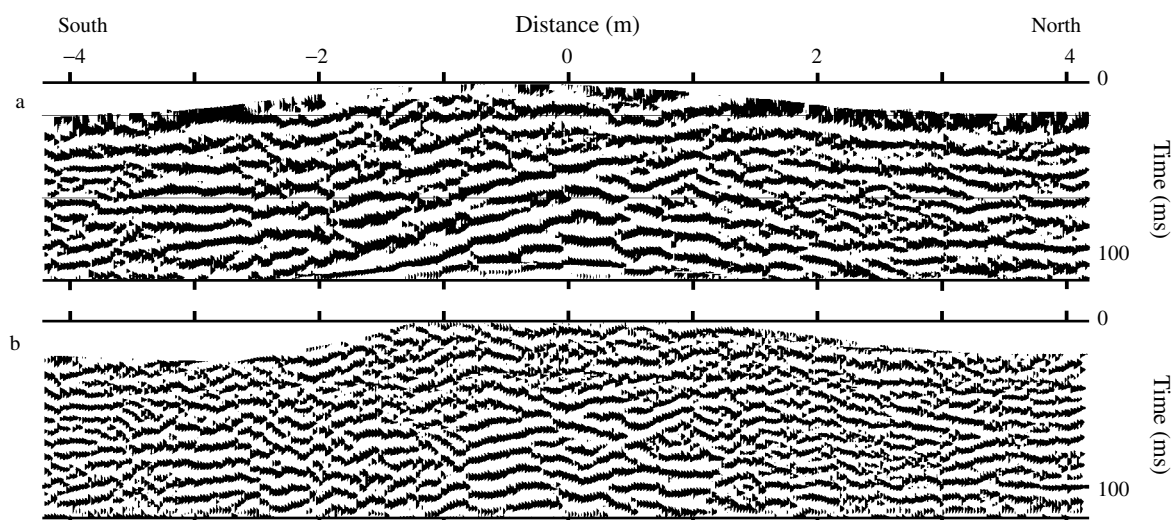


Figure 5. Seismic reflection profile of the CATS burial mound along a north–south profile crossing the mound centre using a hammer source. (a) Band-pass filtered at 100–800 Hz and (b) filtered as above, and frequency–wavenumber migrated assuming  $120 \text{ m s}^{-1}$  velocity.

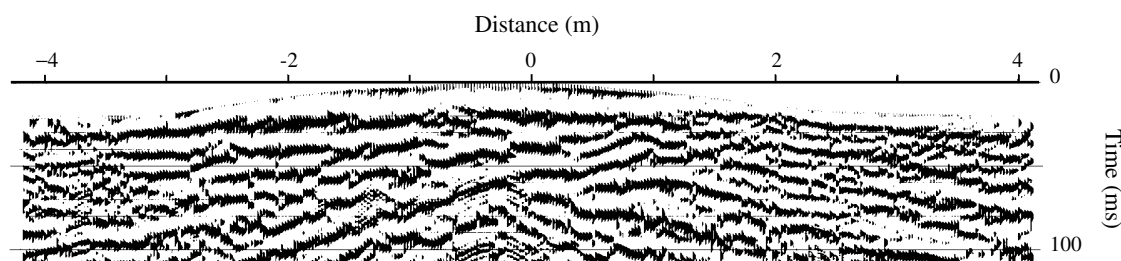


Figure 6. Seismic reflection profile of the CATS burial mound using the vibrator source with a 1–1000 Hz logarithmic sweep. A 10–450 Hz band-pass filter and frequency–wavenumber migration are applied to the image.

In the mound interior, the arrivals have a more triangular shape, dipping more steeply than the mound topography, with an apex beneath the mound summit. The dominance of low-frequency energy, and arrivals with significant lateral energy tails, despite having applied migration, suggests that surface waves may be a dominant mode of propagation for the log sweep vibrating source.

#### Ground-penetrating radar imaging at CATS

A Subsurface Interface Radar (SIR) System-10 manufactured by Geophysical Survey Systems Inc. (GSSI) was used to image the CATS site. The radar antennae have centre frequencies at 500 MHz (GSSI Model 3102A), with a pulse width of 2 ns. Both the transmitting and the receiving antennae are mounted in a single plastic case with dimensions  $18 \times 39 \times 42$  cm and weight 7 kg. A cable connects the SIR-10 to the antenna. To set the radar gain, the antennae were positioned above a prominent deep reflector, and the instrument was allowed to determine an automatic gain curve, using eight gain points over a 30-ns

time window. Once determined, the gain curve was held fixed, and used throughout the entire survey.

The GPR data were collected on a 0.5 m line spacing over the entire CATS site. The SIR-10 unit was positioned at a fixed station as the antenna was pulled directly on the ground surface along 50 m traverses of the site in a north–south direction. Data were collected at walking speed, with fiducial position marks recorded every 1 m along track. Fibreglass measuring tapes were used to mark the tracks; the antenna was pulled adjacent to the tape, with no interference to the radar records. The recording time was 30 ns, and the number of samples per trace was 512. Radar pulses were transmitted at  $62 \text{ scans s}^{-1}$ , and four pulses were stacked for each trace recorded. The resulting record has a trace about every 4 cm along each transect.

In this study, we will focus on the GPR data collected along a single north–south transect crossing the centre of the CATS burial mound. (Three-dimensional processing of the entire CATS GPR data set will be the subject of subsequent research.) To the north–south GPR

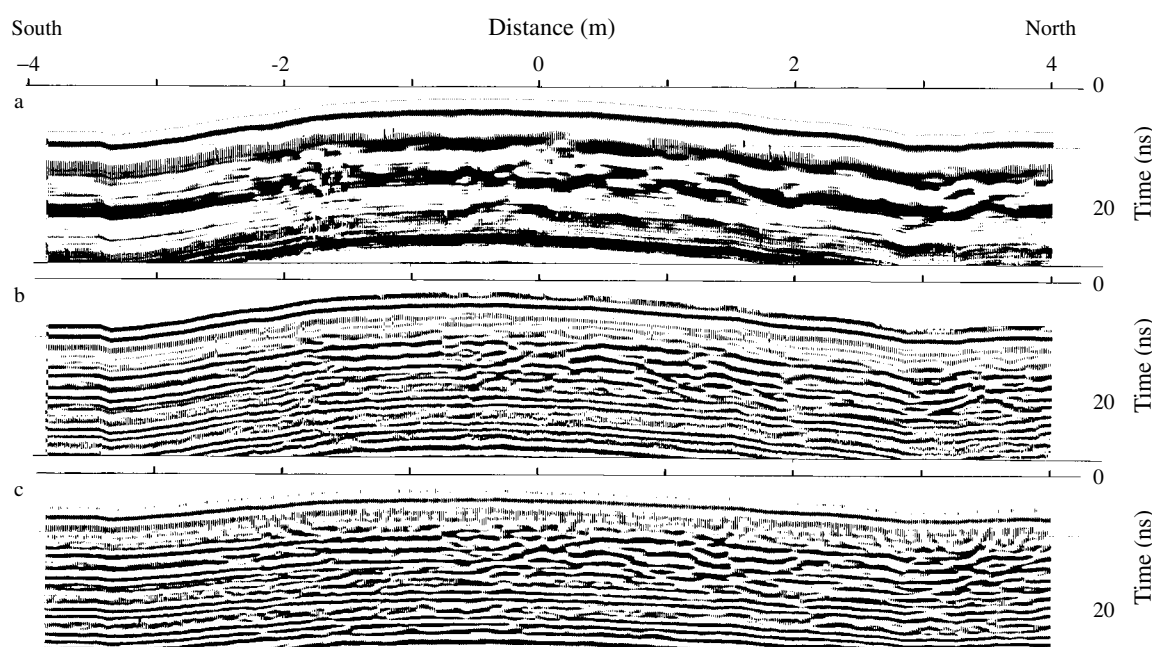


Figure 7. Ground-penetrating radar profile of the CATS burial mound along a north–south line crossing the mound centre (same location as Figure 5 and 6). Data are displayed using a 4 ns AGC window: (a) unfiltered, (b) band-pass filtered for 500–1000 MHz and (c) filtered as above, and migrated assuming a  $170 \text{ mm ns}^{-1}$  velocity.

profile, we applied the mound topography as a static time shift, assuming a  $170 \text{ mm ns}^{-1}$  radar propagation velocity. Figure 7 shows the GPR profile of the burial mound as unfiltered data (a), and as filtered with a band-pass of 500–1000 MHz (b). The unfiltered image (Figure 7a) has a dominant frequency near 200 MHz, at the low frequency end of the 500 MHz centre frequency antennae. The filtered image (Figure 7b) has better definition of features within the burial mound. These images have arrivals that predominantly follow the mound topography throughout the 30 ns data record, suggestive of a 'ringy' source signature. However, the arrivals are disturbed during the time window of 10–20 ns, particularly beneath the mound summit, southern flank, and along its northern edge. Some of these disturbed arrivals appear to be distinct reflectors with hyperbolic shape, for instance, at 0.5 m range and 12 ns time in Figure 7b. Figure 7c shows the filtered GPR data after applying a frequency–wavenumber migration (Stolt, 1978; Hatton *et al.*, 1986) to improve the reflector definition, using a velocity of  $170 \text{ mm ns}^{-1}$ . The hyperbolic reflectors seen in Figure 7b are transformed by migration to be more localized, and in some portions of the image distinct lateral

breaks in the reflecting horizons appear, such as at a range of 1.4 m in Figure 7c. The advantages of migrating even single-channel GPR data have been discussed previously by Fisher *et al.* (1992).

## Discussion

A schematic cross-section of the CATS burial mound at the location of the reflection survey lines is shown in Figure 8a. The key features of the burial mound are: (i) recently disturbed and uncompacted fill forming the mound itself, 1.6 m thick at the centre of the mound; (ii) wood lining along the sides of the burial crypt, extending 1 m in depth; (iii) burial crypt fill; and (iv) burial crypt objects, including the pig, pottery vessels and shells.

The seismic and radar reflection lines are presented along with the burial mound cross-section in Figure 8. Reflections presumed to be from the burial crypt are highlighted in Figure 8b and c. The seismic image produced by the hammer source has strong reflections with good continuity, primarily confined to the region of the burial crypt (Figure 8b). The seismic image within the upper portion of the mound (0–30 ms,

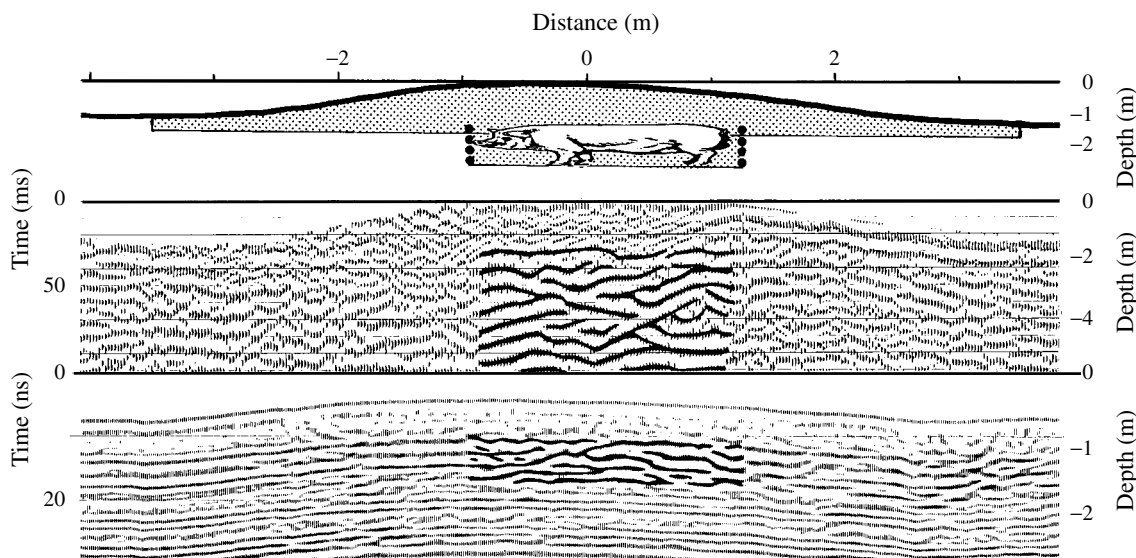


Figure 8. Comparison of known structure with seismic reflection and ground-penetrating radar images. (a) Schematic cross-section of the CATS burial mound along a north–south profile with wood-lined crypt and pig burial. (b) Seismic reflection image (Figure 5b) and (c) ground-penetrating radar image (Figure 7c), with highlighted reflections from the burial crypt.

0–1.8 m) is suggestive of the poorly consolidated and disturbed zone that makes up the mound fill. A series of reflection events in the mound interior corresponds to the location and approximate depth of the central burial crypt. The upper portions of these crypt reflections (30–50 ms, 1.8–3.0 m) are upwardly concave with their centres of concavity in the middle of the crypt. Below the series of concave reflections, strong reflections continue, but they are complex with both flat-lying and dipping events superimposed. It is likely that these events are a result of multiple reflections within the crypt, generated from both the sides and the floor. These complex reflections continue to the full extent of the seismic data (120 ms, 7.2 m), well beyond the bottom of the crypt. A clearly defined lateral break in all these reflections occurs at both sides of the crypt (ranges of –0.9 m and +1.1 m in Figure 8b). Within the mound outside of the crypt region, reflection events are seen, either flat-lying, or dipping away from the edges of the crypt, but they have lesser amplitude and continuity than reflections from within the crypt region (Figures 8b and 5b).

The GPR image (Figure 8c) has a similar character to the seismic reflection image (Figure 8b). In the upper portion of the GPR image (0–10 ns, 0–0.85 m) the data are lineated at the south end of the mound, but reflections are indistinct in the central and northern portions of the mound. This may be due to the disturbed nature of the mound fill, however, comparison of the non-migrated and migrated radar data (Figures 7b and c) suggests some ‘over-migration’ artefacts in the uppermost portion of the image. Beneath the upper zone are a series of reflection events in the mound interior spanning 10–20 ns (0.85–1.7 m). These events correspond well to the lateral location of the central crypt, but they are too shallow by 0.75 m or more. This apparent depth error suggests that our nominal radar velocity of  $170 \text{ mm ns}^{-1}$  may be too slow in the upper portions of the mound. However, the velocity required for a correct depth to the top of the crypt is extremely fast ( $260 \text{ mm ns}^{-1}$ ), approaching the maximum allowed speed of light in vacuum ( $300 \text{ mm ns}^{-1}$ ). In contrast the GPR crypt reflections occupy only the time interval 10–20 ns, correctly giving a depth extent of about 0.85 m.

This suggests that  $170 \text{ mm ns}^{-1}$  is a correct velocity within the lower compacted portions of the mound, consistent with the velocity derived from the migration analysis. A steep velocity decrease with depth, owing to compaction and water saturation, may explain these data. As observed for the seismic crypt reflections beneath the flat or concave upper radar reflections, there are dipping reflectors suggestive of multiple events between the crypt sides and bottom. Lateral reflector breaks occur at both sides of the crypt. Outside of the central crypt region there are suggestions of reflection events at –2 m range; this could be an off-line return from the secondary pig burial (Figure 1). Reflection events are also seen at the northern edge (3 m range) of the mound from an unexplained origin.

The seismic reflection image produced by the vibrating source (Figure 6) is predominantly composed of low-frequency flat-topped triangular arrivals, located beneath the mound summit. These reflections seem to originate from the sides of the burial crypt, perhaps due to surface waves. At higher frequency (360 Hz), however, a well-confined hyperbolic reflection begins at about 45 ms (2.7 m), with its apex located 30 cm south of the mound summit (Figure 6). This is the approximate location and depth of the pig’s chest (Figure 8a). A gas-filled cavity or void within the pig could create a strong energy scatterer, which may be the origin of the 360 Hz reflector. A spherical cavity would resonate when one-quarter of the seismic wavelength matched the cavity radius. For 360 Hz waves travelling in air ( $335 \text{ m s}^{-1}$ ), the cavity radius would be 23 cm, a plausible size for the residual chest cavity of the pig. A similar hyperbolic reflection is seen 1.3 m south of the mound summit at about 65 ms (Figure 6), perhaps corresponding to the secondary pig burial (Figure 1).

## Conclusions

The SRI and GPR images from the CATS burial mound show both similarities and differences in their ability to image subsurface structure. The two imaging techniques applied at this site have energy wavelengths that are comparable to within about a factor of three (GPR at 500 MHz

and  $170 \text{ mm ns}^{-1}$  is  $0.34 \text{ m}$  wavelength, and SRI at  $120 \text{ Hz}$  and  $120 \text{ m s}^{-1}$  is  $1 \text{ m}$  wavelength). The central burial crypt is imaged by both techniques as a flat-lying or concave reflector at the top of the crypt, and as dipping reflectors for greater times, probably related to multiple reflections from the crypt sides and floor. The seismic image provides a good match for the known depth to the top of the crypt; the radar image requires an extremely fast near-surface velocity ( $260 \text{ mm ns}^{-1}$ ), perhaps the result of high porosity in the upper unconsolidated mound fill, with decreasing velocity below. The depth extent of the crypt is best represented by the radar image, which has a series of clear reflectors covering the correct depth range; in the seismic image, reflected energy continues far below the expected depth of the crypt, suggesting multiple reflections within the crypt structure. Complex reflections from the crypt may explain the lack of identifiable reflections from the pig and associated funerary goods.

Reflection imaging techniques have great potential to benefit archaeological field research by allowing, non-destructive prospection, with detailed information on depth as well as lateral extent of buried objects and structures. Application of both seismic and radar imaging to the same site has revealed both similarities and differences in their imaging abilities. The application of these techniques to a site with known features, such as the Controlled Archaeological Test Site, allows ground truth of reflection imaging system performance. The application of multiple reflection methods may allow better understanding of buried archaeological features by providing an independent means for verifying depth, based on the site velocity structure, and by providing multiple images based on common procedures for data filtering, migration and display.

## Acknowledgements

We thank Jon Isaacson, Michael Hargrave, James Zeidler, Eric Hollinger and other members of the United States Army Construction Engineering Research Laboratory staff for providing access to the CATS site. Allan Sauter provided field assistance with the seismic data collection, and Jeff Lucius provided assistance with the radar

data collection. This project was funded by the National Centre for Preservation Technology and Training Grant MT 2210-7-NC-018 under the project management of Mark Gilberg.

## References

- Baker GS, Schmeissner C, Steeples DW, Plumb RG. 1999. Seismic reflections from depths of less than two metres. *Geophysical Research Letters* **26**: 279–282.
- Conyers LB, Goodman D. 1997. *Ground-Penetrating Radar: an Introduction for Archaeologists*. AltaMira Press: Walnut Creek, CA.
- Claerbout JF. 1985. *Imaging the Earth's Interior*. Blackwell Scientific Publications: Oxford.
- Fisher E, McMechan GA, Annan AP, Cosway SW. 1992. Examples of reverse-time migration of single-channel, ground-penetrating radar profiles. *Geophysics* **57**: 577–586.
- France DL, Griffen TJ, Swanburg JG, Lindemann JW, Davenport GC, Trammell V, Armbrust CT, Kondratieff B, Nelson A, Costellano K, Hopkins D. 1992. A multidisciplinary approach to the detection of clandestine graves. *Journal of Forensic Science* **37**: 1445–1458.
- Frazier CH, Cadalli N, Munson DC, O'Brien WD. 2000. Acoustic imaging of objects in soil. *Journal of the Acoustic Society of America* **108**: 147–156.
- Goodman D, Nishimura Y. 1993. A ground-radar view of Japanese burial mounds. *Antiquity* **67**: 349–354.
- Goodman D, Nishimura Y, Rogers JD. 1995. GPR time slices in archaeological prospection. *Archaeological Prospection* **2**: 85–89.
- Isaacson J, Hollinger RE, Gundrum D, Baird J. 1999. A Controlled Archaeological Test Site Facility in Illinois: training and research in archeogeophysics. *Journal of Field Archaeology* **26**: 227–236.
- Hatton L, Worthington MH, Makin J. 1986. *Seismic Data Processing Theory and Practice*. Blackwell Scientific Publications: Oxford.
- Olhoeft GR. 1986. Electrical Properties from  $10^{-3}$  to  $10^9 \text{ Hz}$ —physics and chemistry. In *Proceedings of the Second International Symposium on the Physics and Chemistry of Porous Media*, Bananvar JR, Koplik J, Winkler KW (eds). Held at Schlumberger-Doll Research in Ridgefield, Connecticut on 15–17 October 1986. American Institute of Physics: New York; 281–298.
- Steeples DW. 1998. Shallow seismic reflection section—introduction. *Geophysics* **63**: 1210–1212.
- Steeples DW, Miller RD. 1990. Seismic reflection methods applied to engineering, environmental, and groundwater problems. In *Geotechnical and Environmental Geophysics*, Vol. I, Ward SH (ed.). Society for Exploration Geophysics: Tulsa; 1–30.

- Steeple DW, Miller RD. 1998. Avoiding pitfalls in shallow seismic reflection surveys. *Geophysics* **63**: 1213–1224.
- Stoll RD. 1989. *Sediment Acoustics*. Lecture Notes in Earth Sciences, Bhattacharji S, Friedman GM, Neugebauer HJ, Seilacher A (eds). Springer-Verlag: Berlin.
- Stolt RH. 1978. Migration by Fourier transform. *Geophysics* **43**: 23–48.
- Topp GC, Davis JL, Annan AP. 1980. Electromagnetic determination of soil water content: measurements in coaxial transmission lines. *Water Resources Research* **16**: 574–582.